Materials Today Bio 28 (2024) 101176

Contents lists available at ScienceDirect

Materials Today Bio

journal homepage: www.journals.elsevier.com/materials-today-bio

Biomimetic design and integrated biofabrication of an in-vitro three-dimensional multi-scale multilayer cortical model

Ling Wang [a,b,c,1,*], Luge Bai [a,b,c,1], Sen Wang [a,b,c,1], Jiajia Zhou [a,b,c], Yingjie Liu [a,b,c], Chenrui Zhang [a,b,c], Siqi Yao [a,b,c], Jiankang He [a,b,c], Chaozong Liu [d], Dichen Li [a,b,c,**]

[a] State Key Laboratory for Manufacturing System Engineering, School of Mechanical Engineering, Xi'an Jiaotong University, China
[b] National Medical Products Administration (NMPA) Key Laboratory for Research and Evaluation of Additive Manufacturing Medical Devices, Xi'an Jiaotong University, China
[c] National Innovation Platform (Center) for Industry-Education Integration of Medical Technology, Xi'an Jiaotong University, China
[d] Institute of Orthopaedic & Musculoskeletal, University College London, Royal National Orthopaedic Hospital, Stanmore, UK

ARTICLE INFO

Keywords:
Biofabrication
Brain-like tissue model
Multiscale biomimetic design
Neuron neurite orientation
Fiber topography induction

ABSTRACT

The lack of accurate and reliable *in vitro* brain models hinders the development of brain science and research on brain diseases. Owing to the complex structure of the brain tissue and its highly nonlinear characteristics, the construction of brain-like *in vitro* tissue models remains one of the most challenging research fields in the construction of living tissues. This study proposes a multi-scale design of a brain-like model with a biomimetic cortical structure, which includes the macroscopic structural features of six layers of different cellular components, as well as micrometer-scale continuous fiber structures running through all layers vertically. To achieve integrated biomanufacturing of such a complex multi-scale brain-like model, a multi-material composite printing/culturing integrated bioprinting platform was developed in-house by integrating cell-laden hydrogel ink direct writing printing and electrohydrodynamic fiber 3D printing technologies. Through integrated bioprinting, multi-scale models with different cellular components and fiber structural parameters were prepared to study the effects of macroscopic and microscopic structural features on the directionality of neural cells, as well as the interaction between glial cells and neurons within the tissue model in a three-dimensional manner. The results revealed that the manufactured *in vitro* biomimetic cortical model achieved morphological connections between the layers of neurons, reflecting the structure and cellular morphology of the natural cortex. Micrometer-scale (10 μm) cross-layer fibers effectively guided and controlled the extension length and direction of the neurites of surrounding neural cells but had no significant effect on the migration of neurons. In contrast, glial cells significantly promoted the migration of surrounding PC12 cells towards the glial layer but did not contribute to the extension of neurites. This study provides a basis for the design and manufacture of accurate brain-like models for the functionalization of neuronal tissues.

1. Introduction

Understanding and developing neural tissues is a frontier direction for future life science research. However, due to ethical constraints, the scarcity of models available for brain science and brain disease research remains an urgent problem in the development of brain science. Therefore, the development of *in vitro* living tissue models that can replicate natural brain neural tissue has become a hot topic and frontier research field in current brain science research. Neural tissue is a complex and highly nonlinear system [1], containing nearly one hundred billion nerve cells forming complex and specific neural networks through hundreds of trillions of connections [2]. This tissue is characterized by significant multi-scale and multi-cellular features, with a distinct six-layer structure at the macro scale, and multiple types of neural cells contained within each layer at the micro scale. Moreover, neurons between different layers have distinctively oriented connection features, and the orientation growth of neuronal neurites forms specific topological connection networks. Therefore, constructing brain tissues

* Corresponding author. School of Mechanical Engineering, Xi'an Jiaotong University, Xi'an, 710054, Shaanxi, China.
** Corresponding author. School of Mechanical Engineering, Xi'an Jiaotong University, Xi'an, 710054, Shaanxi, China.
E-mail addresses: menlwang@mail.xjtu.edu.cn (L. Wang), dcli@mail.xjtu.edu.cn (D. Li).
[1] These authors contributed equally to this work.

https://doi.org/10.1016/j.mtbio.2024.101176
Received 6 April 2024; Received in revised form 1 July 2024; Accepted 29 July 2024
Available online 2 August 2024

in vitro is one of the most challenging research areas in the construction of living tissue models. The main difficulties to this include the multi-scale integrated manufacturing of complex brain tissue structures and achieving specificity and directionality in the distribution of multi-level and multi-cellular structures in the tissue.

In the fields of biomanufacturing and tissue engineering, existing in constructing brain-like models *in vitro* has mostly employed two-dimensional (2D) planar culture platforms, microfluidic chips, and lithography techniques for the i*n vitro* preparation of biomimetic neural networks. This has achieved the precise fabrication of neural circuits at a certain level and precise placement of cells with micrometer-or even nanometer-scale accuracy, as well as the unidirectional connection of neural axons. However, much of this research is limited to 2D or 2.5D functional connections, and cannot simulate the three-dimensional (3D)-oriented connections of natural neural tissue [3]. Preliminary studies have investigated the interactions between neurons and glioma cells in a 3D brain glioma model prepared *in vitro* [4], demonstrating that 2D planar cultures cannot replicate, but exist in vivo. Therefore, the *in vitro* construction of 3D brain-like neural tissues is an inevitable developmental direction in brain science.

The current manufacturing techniques for *in vitro* 3D brain-like tissue models primarily involve cell biology and tissue engineering technologies. Common cell biology methods involve the induction of neural cells *in vitro* to form 3D spheroids [5] or organoids [6]. For instance, Gonzalez et al. [7] used iPSCs from patients with Alzheimer's disease (AD) to induce the formation of 3D brain-like organoids *in vitro*, and Shoji Takeuchi et al. [8] constructed Neural Building Blocks (NBBs) that form functional neural networks based on the self-assembly of rat cortical cell spheroids. However, the development of 3D models manufactured using this technique is limited because of restricted nutrient transfer. Traditional tissue-engineering methods simulate specific brain tissue structures using scaffolds [9], microfluidic platforms [10], or lithography techniques. For example, Chwalek et al. [9] created simple gray and white matter structures using concentric ring scaffolds and cell perfusion based on a molding method, whereas Bang et al. [10] constructed a simplified 3D neuronal circuit microfluidic model to simulate the dynamics of neurite outgrowth along the extracellular matrix fibers. Tissues manufactured using this method are limited by their uniform composition and structure, making it difficult to achieve the layered and oriented complex structures of the brain cortex.

In tissue engineering and biomanufacturing, 3D printing technology offers a new pathway for constructing complex structural models of brain-like tissues. This allows for the precise allocation of biomaterials such as cells and growth factors, and the creation of complex 3D structures that encapsulate cells. At the same time, it provides strict spatial regulation of cells and signaling factors, enabling the manufacture of complex tissue structures with multi-cellular systems and multi-scale dimensions. Bioprinting technologies include extrusion, inkjet, photopolymerization, and laser-assisted bioprinting [11,12]. Among these, direct ink writing (DIW) has become the most widely used bioprinting method because of its cell friendliness. Song et al. [13] used the DIW method to construct a brain-like biomimetic tissue with uniform layered structures and network morphologies. Lozano et al. [14] used a hand-held extrusion nozzle to build a three-layered brain-like tissue structure containing cortical neurons. Li et al. [15] developed a heterogeneous 3D brain-like co-culture model with neuronal spheroids and glial cells based on the suspended extrusion technique. These studies have simulated the microenvironment of the human brain in vivo to some extent but the constructed tissues are still limited to small sizes, single-cell types, and simple structural models, and cannot manipulate cell orientations. The existing literature indicates that microfibers produced by electrospinning technology, on a scale smaller than or close to the size of cells, can affect the adhesion, migration, and neurite outgrowth of neural cells [16–18]. Hajiali et al. [19] discovered that polyphenylsulfone (PPSu) electrospun polyphenylsulfone nanofibers supported the adhesion and differentiation of neural stem cells. In contrast, electrohydrodynamic (EHD) technology can precisely control the deposition location of the fibers. Chen et al. [20] printed a polycaprolactone scaffold with ultrafine fibrous heterogeneous structures for directed growth regulation of neuron-like PC12 cells. Lee et al. [21] found that embedding PCL fibers printed via EDH significantly increased the axon length of neurons in the hydrogel and extended the axons along the fibers. Tissue structures that combine high-precision fibers with biocompatible hydrogel printing exhibit excellent performances. However, this indirect manufacturing method, which prints scaffolds before combining them with cells, was found to be difficult to achieve precise manufacturing of layered tissues.

Cell lines derived from tumors, such as PC12 and GL261 cells, offer a cost-effective and adaptable solution for neurobiological research, and are widely used in in-vitro studies of neurological diseases. Studies have shown that PC12 cells have a reversible neuronal phenotype response to nerve growth factor (NGF), making them suitable as a model for neuron cells after pre-differentiation [16]. Although the PC12 cell line is not a model for cortical phenotype, due to its ability to secrete catecholamines, especially dopamine, and respond to NGF, PC12 cells have been used as model cells for diverse studies on neurosecretion [22] and Parkinson's disease [23].

In this study, a biomimetic six-layer multi-cellular 3D tissue model mimicking the natural brain cortex was proposed. A bioprinting ink material system that is both printable and suitable for the growth of neural cells was developed and a multi-material composite printing/culturing integrated printing platform was built in-house. Based on this, an integrated 3D printing process involving both cell-laden hydrogel DIW printing and EHD fiber printing technologies was developed and used to manufacture biomimetic brain-like 3D tissue models. Furthermore, the impact of the structural parameters of the fiber and the manufacturing processes of the hydrogel/fiber composite on cell behavior within the tissue was systematically investigated.

2. Materials and methods

2.1. Biomimetic design of cortical tissue model

The natural brain cortex comprises a six-layer structure composed of neurons and astrocytes (Fig. 1a) and the morphology, distribution, and function of neurons vary across the layers. The first layer was primarily composed of horizontally aligned cells, whereas the cells in the second to sixth layers were mostly arranged in a cross-layer vertical alignment. Based on these structural characteristics, a biomimetic cortical model that simulates the natural cortical structure was designed (Fig. 1b). The model had a thickness of 3 mm and was uniformly divided into six layers, labeled Layers I–VI. Layer I, which is also the top layer, contains uniformly distributed horizontal fibers that guide the cells to spread in the horizontal direction. Layers II–VI contain uniformly distributed vertical cross-layer fibers that guide the vertical orientation of neuronal neurites. This model employs alternating printing of PC12 and GL261 cell lines to verify the controllability of cell distribution proposed by this manufacturing method and allows for a more intuitive observation of the interactions between these two types of cells within 3D multilayered tissues *in vitro*. Furthermore, a six-layer multi-cellular tissue without fibers was established as a control model, CT1 (Fig. 1c), to compare the value of having fibers present. Another control model, CT2 (Fig. 1d), including fiber structures without the six-layer structure supporting cell layers, was constructed to study the interactions between the two types of cells.

2.2. Materials and Equipment

Cell source: The PC12 cells (low-differentiation) used in this study were purchased from the Cell Bank of the Chinese Academy of Sciences (TCR 8, National Collection of Authenticated Cell Cultures, China), and GL261 cells expressing green fluorescent protein (GFP) were acquired from Shanghai Zhongqiao Xinzhou Biotechnology Co., Ltd. All cell-laden

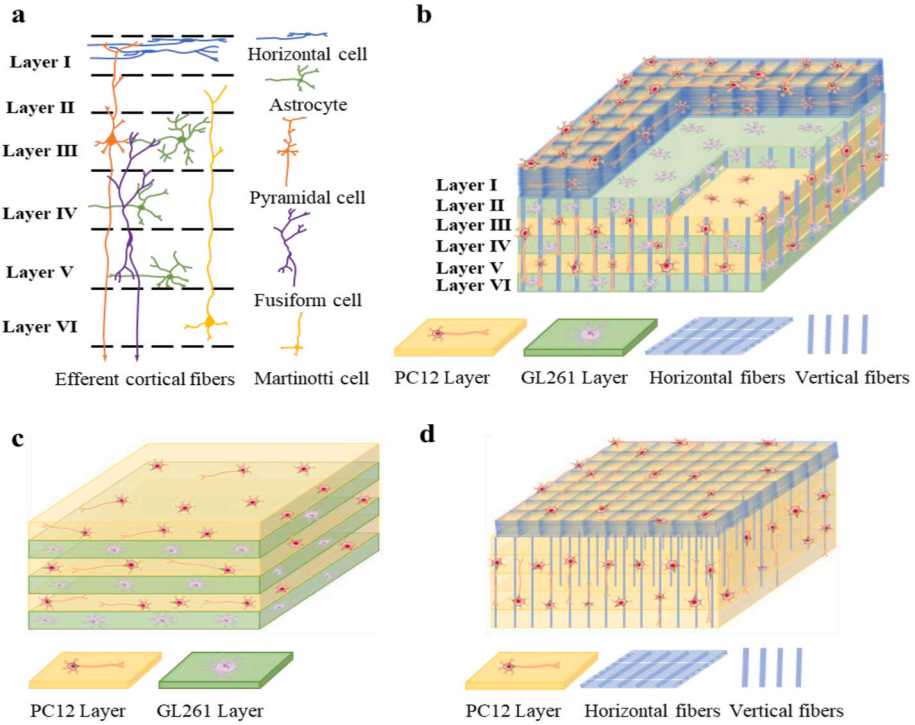

Fig. 1. Diagram of the designed biomimetic cortical model. (a) The six-layer structure and cell distribution of the natural cerebral cortex; (b) The six-layer structure of the designed model (T); (c) The control model (CT1) without fiber contents; (d) The control model (CT2) without GL261 cells.

tissues were cultured using a complete culture medium: 89 % [v/v] high-glucose Dulbecco's Modified Eagle Medium (DMEM, Hyclone), 10 % [v/v] fetal bovine serum (FBS, Gibco), 1 % [v/v] penicillin/streptomycin (P/S, Hyclone), and 50 ng/mL nerve growth factor, with the culture medium replaced every 48 h.

Bioink: Methacrylated gelatin (GelMA, EFL-GM-PR-002) mixed with fibrinogen was selected as the matrix material for cell printing. GelMA exhibits good molding properties under the influence of ultraviolet or visible light [3,24] and is suitable for the growth and differentiation of neural cells [25]. Additionally, fibrinogen (Fib) was mixed with GelMA to form fibrin monomers under the action of thrombin, which further formed stable fibrin polymers under the influence of Ca^{2+} [26]. This process effectively promotes cell proliferation, migration, and differentiation. Therefore, the GelMA solution combined with Fibs formed a dual-network hydrogel material through a two-step cross-linking process involving light and ions, which is conducive to the spreading of neural cells. Fib powder (Sigma-Aldrich) was dissolved in saline and incubated at 37 °C for 2 h to obtain a 3 % [w/v] Fib solution. Lyophilized GelMA (from EFL company) spongy solid was dissolved in saline and magnetically stirred at 300 rpm at 37 °C for 1 h, yielding a 7.5 % [w/v] GelMA solution. Subsequently, at 37 °C, the Fib solution and GelMA solution were mixed to obtain the GelMA/Fib solution, which was then sterilized using a 0.22 μm filter. Six different concentrations of GelMA/Fib solutions were prepared, named G5 (5 % w/v GelMA), G7.5 (7.5 % w/v GelMA), G10 (10 % w/v GelMA), G5F0.5 (5 % w/v GelMA and 0.5 % w/v Fib), G5F1.0 (5 % w/v GelMA and 1.0 % w/v Fib), and G5F1.5 (5 % w/v GelMA and 1.5 % w/v Fib), for the optimization of the mixing ratio of the two contents. After thawing from a frozen state, PC12 cells and GL261 cells were respectively cultured in petri dishes until they reach 80 % confluence. The cells were then digested and centrifuged to form a cell suspension for later use. Then, PC12 and glial cells were added to the GelMA/Fib solutions at densities of 4 × 10^6 cells/mL and 2 × 10^6 cells/mL, respectively, to obtain cell-loaded bioprinting inks.

3D Printing Equipment: A self-developed multimaterial composite printing/culturing integrated 3D printing platform (Fig. 2a) was used in this study, which included four functional modules: a 3D moving platform, multi-nozzle extrusion printing module, melt electrospinning writing module, and environmental control module. The 3D moving platform has a repeat positioning accuracy of ±5 μm in the XY direction and ±10 μm in the Z direction. The multinozzle extrusion printing module, driven by pneumatic pressure, can achieve 3D printing of hydrogels with different viscosities and molding methods. The melt electrospinning writing module operates with either micro-injection pumps or pneumatic pressure as the driving force, with a maximum heating temperature of 200 °C, enabling the printing of fibers at both the micro- and nanoscales. The environmental control module includes air filtration and ultraviolet sterilization devices and integrates multi-parameter controls for temperature (0–45 °C), humidity (45 %–95 % RH), oxygen concentrations (1–99 %), and carbon dioxide concentrations (0–20 %), ensuring an average cell survival rate greater than 95 % after cell printing.

2.3. 3D printing process

GelMA/Fib DIW Printing Process: The ink-printing process includes three stages: pretreatment (pre-cooling at low temperature), 3D printing, and post-treatment (photocuring and ion crosslinking), as illustrated in Fig. 2b. Pretreatment involves the process of precooling the mixed ink in a 4 °C refrigerator for 15 min before printing due to its low viscosity, which allows GelMA to preliminarily gelatinize before 3D printing is conducted in an environmental control chamber. During the printing process, the temperature of the printer was controlled at 24 °C, humidity at 50 % RH, and CO_2 concentration at 5 %. The printing parameters are shown in Table 1, and the printing resolution is 425.56 ± 73.62 μm. The post-treatment involved curing the printed tissue blocks under a UV light source for UV light-induced crosslinking (15 s) to solidify GelMA in the matrix, followed by chemical crosslinking solidification of fibrinogen using crosslinking agents (0.2 % w/v $CaCl_2$ and 10 U/mL thrombin) in an incubator for 2 h. Finally, the tissue blocks were cultured in a complete culture medium with regular medium changes and observations.

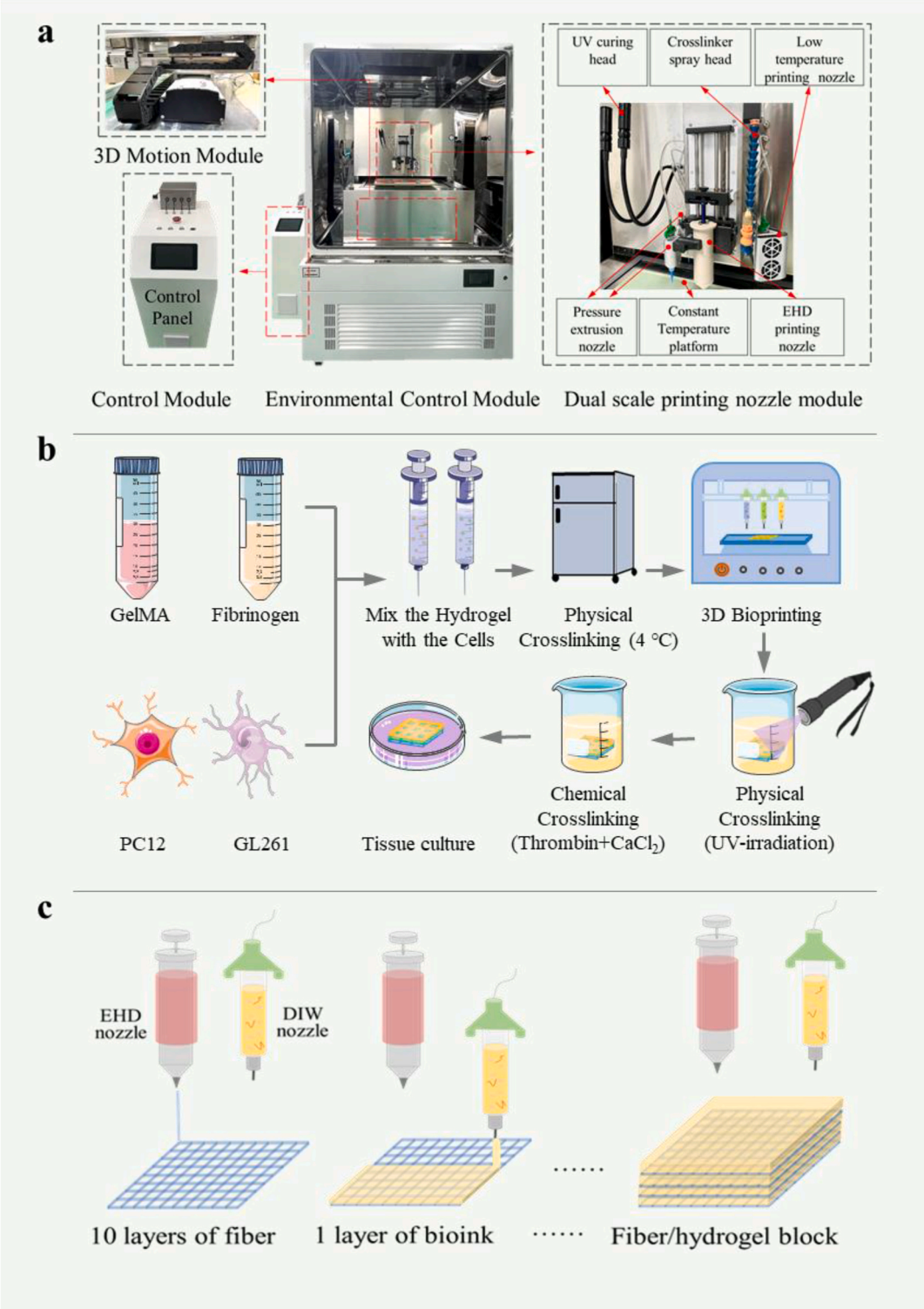

Fig. 2. (a) 3D printing platform; (b) Diagram of printing procedure for the GelMA/Fib composite tissue block; (c) Diagram of printing procedure for the hydrogel/fiber composite tissue structure.

Table 1
Printing parameters.

Project	Air pressure (mbar)	Movement speed(mm/s)	Receiving distance (μm)	Voltage (kV)	Printhead temperature (°C)
DIW	320	10	100	–	24
EHD	30	20	4000	4	90

Manufacture of Hydrogel/Fiber Composite Structures: First, a layer of bioink with a thickness of 400 μm was printed using a DIW printhead loaded with bioink. Then, an EHD printhead loaded with polycaprolactone (PCL, Jinan Daigang Biomaterial Co., Ltd.) was used to print ten layers of PCL fibers (total thickness of 100 μm). The printing parameters are shown in Table 1, and the printing resolution of EHD is 9.37 ± 1.31 μm. This alternating process was repeated until the

thickness of the target tissue was reached (Fig. 2c).

Using the abovementioned printing method, hydrogel/fiber composite tissues with a fiber spacing of 300 μm and various fiber diameters (D10, D30, and D60 represent 10, 30, and 60 μm diameter), were prepared to study the impact of fiber diameter on cell orientation. Using the same manufacturing method, hydrogel/fiber composite structures with a selected fiber diameter of 10 μm and different fiber spacings (S150:150 μm, S300:300 μm, and S500:500 μm) were printed to investigate the effect of fiber spacing parameters on cell orientation. The printed tissues were cultured in a complete culture medium in an incubator before they were subjected to immunofluorescence staining, followed by measurement and statistical analysis of the length of neurites within the tissues and the angle of orientation relative to the fibers (N = 4).

Printing of the Six-Layer Brain Cortex Model: In the six-layer biomimetic brain cortex model designed in this study, the continuous fibers in layers II to VI run longitudinally through each layer, differing from the horizontal direction of the first layer; thus, an indirect printing procedure was developed to fabricate the complete model. First, the DIW method was used to print layers II–VI of the model, where each layer was printed with two types of bioinks using two hydrogel DIW printheads operating in parallel with alternating layer thickness parameters, and each layer was interlaid with horizontally aligned continuous fiber structures. This structure was then rotated 90° around the y-axis via a pre-prepared clamp to transform the originally horizontally laid fibers into a direction that vertically penetrated the layers. Finally, after repositioning, the top layer was printed on top of the model with a continuous horizontally oriented fiber (Fig. 3).

2.4. Histological studies

Live/Dead Staining: The viability of cells in the printed tissue blocks of group G5, G7.5, G10, G5F0.5, G5F1.0, and G5F1.5 was assessed on days 2, 4, and 6 of culture using the LIVE/DEAD® Viability/Cytotoxicity Kit (L3224, Thermo, USA); the long-term cell viability of the G5F0.5 group was evaluated on days 12, 18, 24, and 30 of culture. Live cells are marked with green fluorescence and dead cells are marked with red fluorescence. Fluorescence images of the cells were obtained using a Laser Scanning Confocal Microscope (LSCM; A1, Nikon, Japan). ImageJ software was used to count live and dead cells. Cell viability was quantified as the ratio of green cells to the total number of cells (N = 4).

Immunofluorescence Staining: Tissue blocks were fixed in 4 % paraformaldehyde solution for 2 h and then washed three times with PBS, each time for 15 min. Before staining, the blocks were frozen and sliced in direction parallel to the fiber printing plane with a slice thickness of 100 μm. Specifically, for the final cortical models, the slicing direction was parallel to fibers in Layers II-VI. Beta-III tubulin primary antibody (Abcam) was diluted to 1:200 in a mixture of 5 % goat serum (AR0009, Boster, USA) and 0.3 % Triton X-100 (T8200, Solarbio) and used to incubate the samples overnight at 4 °C. After incubation, the samples were washed thrice with PBS for 15 min each. Alexa Fluor 594 secondary antibody (Abcam) was diluted 1:200 in 5 % goat serum and incubated for 4 h. Finally, after incubation with DAPI (Solarbio) for 20 min, the samples were washed three times with PBS for 15 min each. Samples were observed under LSCM, z-stacks of 100 μm in height were flattened, and cell morphology was characterized using ImageJ software (N = 4).

2.5. Mechanical test for printed samples

Hydrogel blocks with dimensions of 6 × 6 × 5 mm were printed for all groups according to their material content (G5, G7.5, G10, G5F0.5, G5F1.0, and G5F1.5) (N = 4). A universal testing machine (ETM103A; Shenzhen Wansi Test Equipment Co., Ltd., China) was used to perform static compression tests on each tissue block specimen. The experiment was set at a compression speed of 2 mm/min, stroke of 2.55 mm, and load of 50 N. The hydrogel blocks were placed on the testing platform, and the loading head was slowly moving towards until touching the upper surface of the blocks, that was the instance that the data collection began, and the stress-strain curves for all test groups were recorded. To characterize the mechanical properties of each hydrogel block, the compression modulus of each group was derived from the linear phase of the curves.

2.6. Microstructure characterization of the printed tissue

Hydrogel blocks with dimensions of 10 × 10 × 2 mm were printed according to the material content of each test group (G5, G7.5, G10, G5F0.5, G5F1.0, and G5F1.5) (N = 4). After soaking in ultrapure water for 2 min, the hydrogel blocks were dried with absorbent paper, freeze-dried for 44 h using a vacuum freeze dryer (VFD2000; BIOCOOL, China), and then sputter-coated with gold. The surface microstructures of the samples were observed using a Scanning Electron Microscope (SEM, SU-8010, Japan), from which ten pores of each block were randomly selected and measured using AutoCAD software to determine the average pore size (N = 4).

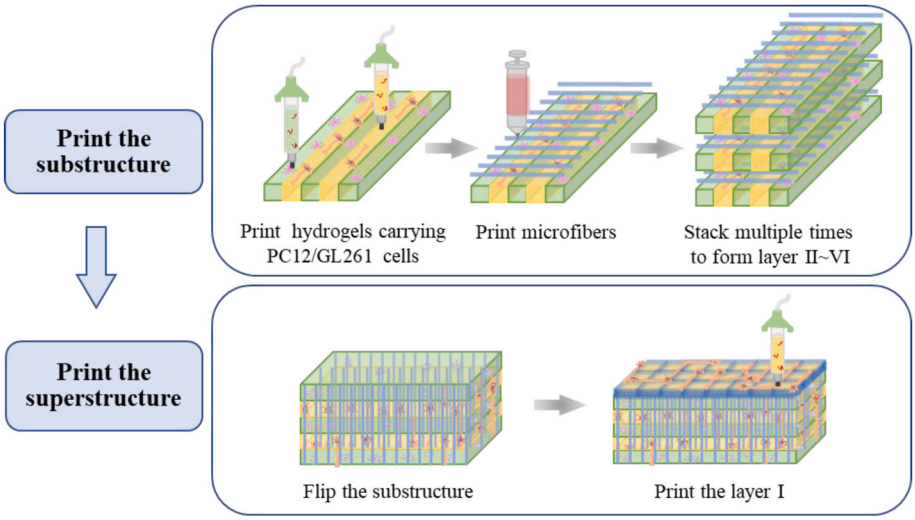

Fig. 3. Diagram of 3D printing procedure for the six-layer brain-like tissue model.

2.7. Statistical analyses

Statistical analyses were performed using GraphPad Prism 9. Differences in the mechanical properties and micropore sizes of the samples were analyzed using one-way ANOVA. Differences in cell viability among all groups were analyzed using two-way ANOVA, with results presented as mean ± standard deviation (SD). The significance levels are denoted as * ($p < 0.05$), ** ($p < 0.01$), and *** ($p < 0.001$).

3. Results

3.1. Mechanical properties of the GelMA/Fib composite tissue blocks

3.1.1. The effect of GelMA

The compression moduli of the GelMA hydrogel blocks printed with different GelMA concentrations are shown in Fig. 4a. The modulus of the hydrogel blocks significantly increased with an increase in the concentration of GelMA and the compression modulus of the G5 group (8.48 kPa) was closer to the modulus of natural cortical tissue (several hundred to a few kPa). The microstructure of the samples was imaged after freeze drying. The results showed that the GelMA hydrogel blocks in all groups contained uniformly distributed micropores with smooth walls (Fig. 4b) and the sizes of these micropores gradually decreased with increasing GelMA concentration (Fig. 4c). After 6 days of culture, the PC12 cells encapsulated in all groups maintained a spherical morphology (Fig. 4d) and the cell survival rate exceeded 85 % (Fig. 4e). These results indicated that the GelMA content in the matrix material did not significantly affect the survival rate of PC12 cells. Based on these findings, a GelMA concentration of 5 % was selected for further experiments.

3.1.2. The effect of Fib concentration

GelMA/Fib hydrogel blocks with different Fib contents were prepared by printing with 5 % (w/v) GelMA. The results indicated that an increase in the Fib content significantly reduced the compressive modulus of the tissue blocks (Fig. 5a), with G5F1.5 showing the lowest modulus (1.67 kPa), whose flowability was too high to be used for printing. The microstructure of the samples was imaged after freeze drying. Under an electron microscope, submicron-level pores were observed in the micropore walls of the GelMA/Fib hydrogel blocks. As the Fib content increased, the micropore walls became thicker and rougher (Fig. 5b). The micropore size decreased with increasing Fib concentration, with G5F0.5 having a pore size (237.18 μm) the closest to the mass transfer requirements of natural brain tissue (Fig. 5c). The cytological experiment results showed that the morphology of PC12 cells could be improved with an increase in Fib content, with the G5F0.5 group showing the best cell morphology (Fig. 5d). During the 6 days of culture, the survival rate of PC12 cells in all groups remained above 85 % (Fig. 5e), indicating that Fib content had no significant effect on cell viability. Considering these findings, a concentration of 5 % GelMA and 0.5 % Fib was selected as the matrix material for constructing the biomimetic cortical model in this study. During the 30-day culture period, the shape of the GelMA/Fib hydrogel blocks was well preserved and the survival rate of PC12 cells within the tissue blocks remained consistently above 85 % (Fig. 5f and g).

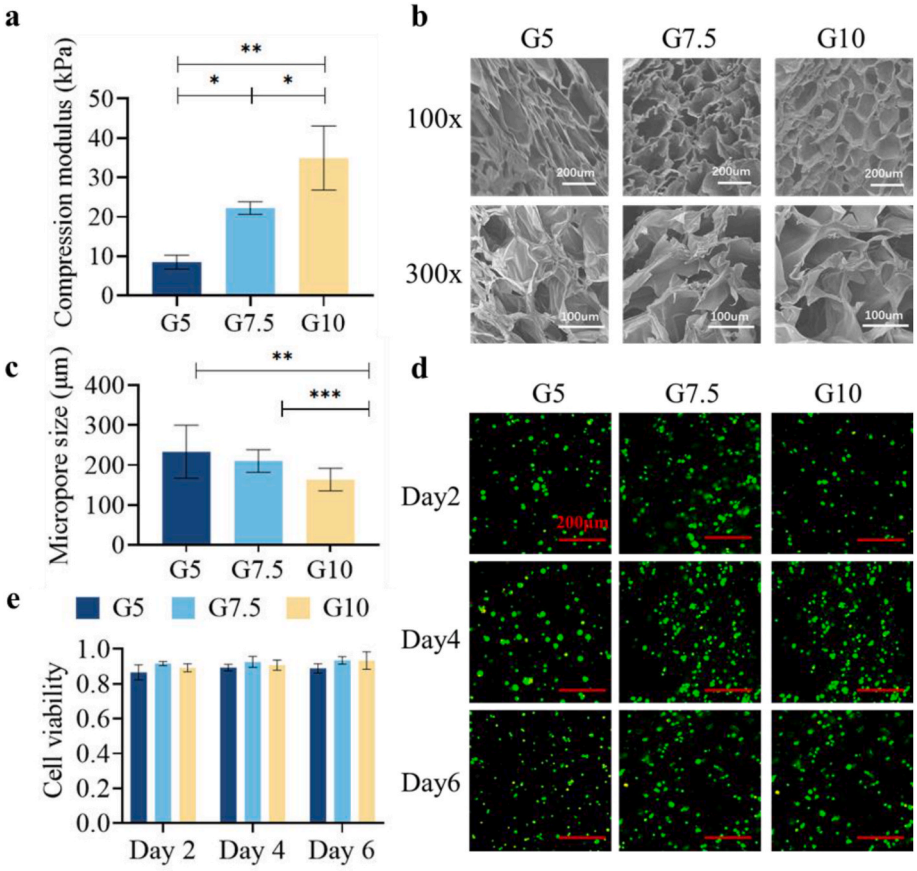

Fig. 4. The effect of GelMA contents on the properties of the composite GelMA/Fib tissue blocks. (a) Compressive modulus for the group of G5, G7.5 and G10; (b) The SEM images of the group of G5, G7.5 and G10; (c) The pore sized of group G5, G7.5 and G10; (d) The Live/Dead images of groups G5, G7.5 and G10 (green: Live; red: Dead); (e) The cell viability of PC12 in group of G5, G7.5 and G10 after 2 day, 4day and 6 days of culture; (one-way ANOVA was used in a and c, two-way ANOVA was used in e; error bar stands for standard deviation (SD); *$p < 0.05$, **$p < 0.01$, ***$p < 0.001$, ****$p < 0.0001$).

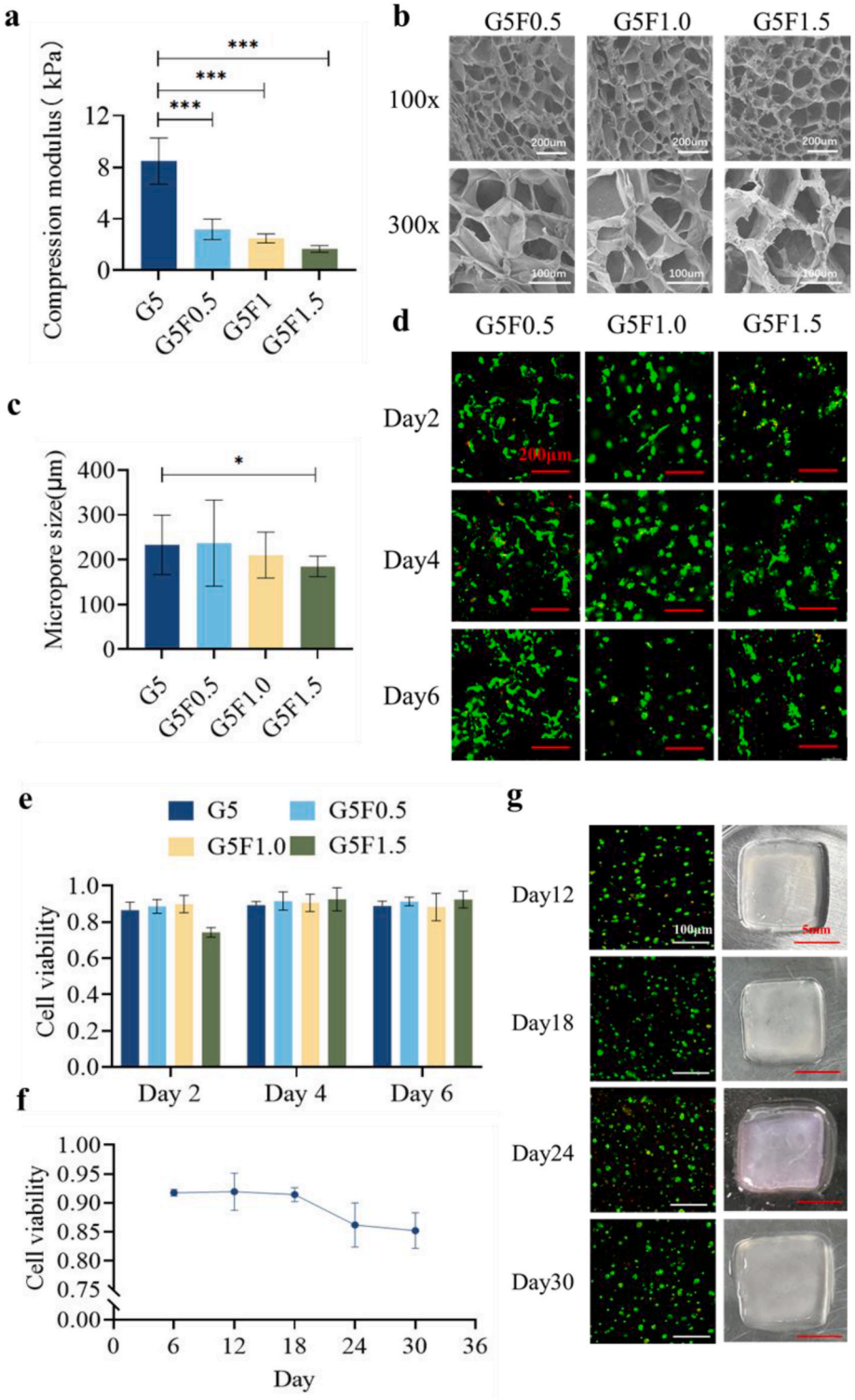

Fig. 5. Effect of Fib concentration on the mechanical properties of the GelMA/Fib composite hydrogel tissue blocks. (a) Compressive modulus of group G5, G5F0.5, G5F1.0 and G5F1.5; (b) SEM images of group G5F0.5, G5F1.0 and G5F1.5; (c) Micropore sizes for group G5, G5F0.5, G5F1.0 and G5F1.5; (d) The Live/Dead images of groups G5F0.5, G5F1.0 and G5F1.5 (green: Live; red: Dead); (e) The cell viability of PC12 in group of G5F0.5, G5F1.0 and G5F1.5 after 2 day, 4day and 6 days of culture; (f) The long term cell viability of PC12 in group G5F0.5 during 30 days of culture; (g) The Live/Dead images and photos of group G5G05 during 30 days of culture (one-way ANOVA was used in a and c, two-way ANOVA was used in e; error bar stands for standard deviation (SD); *$p < 0.05$,**$p < 0.01$,***$p < 0.001$,****$p < 0.0001$).

3.2. Effect of fiber structural parameters on cell orientation

3.2.1. Effect of fiber diameter on cell orientation

The manufactured tissue blocks with consistent thickness but containing fibers of different diameters (10, 30, 60 μm) (N = 4) were observed under a laser confocal microscope for cell morphology and the evaluation of cell orientation after undergoing tissue culture and histological staining. Neurites with angles $\leq \pm 15^{\circ}$ relative to the fibers

(both horizontally and vertically) were defined as oriented neurites, while others were defined as non-oriented neurites, based on that both the angles and length were counted for each neurite and statistical analyses were carried out. The results, as shown in Fig. 6, indicated that in all groups, neurites close to the fibers were longer than those in other locations. In D10, the neurites and cell bodies tightly followed the microfibers. In D30 and D60, most cells were spherical with randomly extending neurites and only a few cells exhibited a clear orientation. After 6 days of culture, the total length of neurites in the D10 group (~250 μm) was significantly longer than those in the D30 and D60 groups. The orientation rate, expressed as the ratio between the orientated neurites over the total number of neurites, in D10 was higher than those in D30 and D60, reaching nearly half (47.59 % ± 1.4 %), and the smaller the angle between the neurite and the fiber, the longer its length becomes. Therefore, it is evident that in the hydrogel/fiber composite structures manufactured in this study, fibers with a smaller diameter (10 μm) are more effective in guiding neurite growth.

3.2.2. The effect of fiber spacing on cell orientation

Tissue blocks with a fiber diameter of 10 μm but varying fiber spacing parameters (150, 300, 500 μm) were prepared, cultured, and histologically stained (N = 4). As described above, neurite orientation was statistically analyzed. The results indicated that in all groups, the neurites of cells close to the fibers tended to extend along the nearest fiber, whereas neurites for the other cells extended randomly (Fig. 7). Additionally, the neurites of the PC12 cells close to the fibers were longer than those far from the fibers. The neurite lengths in S300 and S500 were significantly longer than those in S150, with the maximum length reaching over 250 μm, whereas the neurites in S150 were relatively short, with only a few reaching 150 μm. However, the proportion of oriented neurites in S150 was 61.73 % ± 1.92 %, higher than that in S300 (52.54 % ± 0.8 %) and S500 (49.2 % ± 1.96 %). In the hydrogel/fiber composite tissue blocks, fibers with a diameter of 10 μm and spacing of 150 μm performed the best in terms of neurite orientation guidance. Therefore, a hydrogel/fiber composite structure with a diameter of 10 μm, longitudinal spacing of 150 μm, and lateral spacing of 750 μm was manufactured in the subsequent studies and the purpose of setting larger lateral fiber spacing is to ensure the stability of the fiber scaffold.

3.3. Morphological studies for the printed biomimetic cortical model

The printed biomimetic cortical model (T) and the two control groups (CT1 and CT2) displayed a six-layer structure from both macroscopic and microscopic perspectives (Fig. 8). In the T and CT1 groups, two types of cells were printed in layers, resulting in clear boundaries between the PC12 and GL261 layers in these two structures. This was not the case in the CT2 group, as the latter consisted of a single-cell type. Distinctive cross-layered fiber structures were observed in the T and CT2 groups, whereas there was no continuous fiber distribution in the CT1 group. Tissue staining results indicated that cell migration occurred in the CT1 and T (encapsulating GL261 cells) groups, with PC12 cells migrating into the GL261 cell layer; however, no migration from GL261 to the PC12 layer was observed. In the T group, the presence of fibers played a guiding role in the migration of PC12 cells in the tissue block, with about 87 % of PC12 cells growing 1–2 neurites that extended along the fibers, reaching a maximum neurite length of 200~300 μm. Notably, in the T group, PC12 cells extended their neurites into the GL261 cell layer, with GL261 cells adopting an elongated spindle shape along the fibers rather than a spherical shape as shown in the CT1 group, where the neurites of PC12 cells were fewer, shorter (about 20~30 μm), and extended randomly.

4. Discussion

In this study, we proposed a multi-scale, multi-cellular, and biomimetic cortical brain model. This model integrates the structural and morphological characteristics of the natural brain cortex, such as multi-cellular stratified heterogeneous distribution and continuous fiber cross-layer distribution, providing a foundational model for simulating the multilayered and multi-cellular distribution of the natural brain cortex, as well as cell orientation and interlayer communication between cells. To fulfill the manufacturing demands of such biomimetic tissue models, we developed a low-modulus, printable biomaterial ink tailored for the *in-vitro* construction of brain-like tissue, systematically studied the impact of different components in the bioink on post-printing tissue performance and optimized the ink composition. A coupled 3D bioprinting technique that integrates ink extrusion and fiber electrostatic writing processes was proposed to achieve the integrated direct printing and manufacturing of hydrogel tissues with composite continuous fiber structures. The impact of fiber dimensional parameters on the orientation of neural cells in postprinted tissues was systematically studied, and optimized processes and design parameters were developed. Finally, the designed multilayered, multi-cellular, and complex topological structures of the brain-like cortical tissues were printed using an integrated printing technique. Within the manufactured *in-vitro* biomimetic cortical model, morphological connections between neurons across the layers were achieved, reflecting, to a certain extent, the structure and cellular morphology of the natural cortex.

Owing to the extremely low modulus of natural brain tissue, a matrix bioink for brain-like tissue printing should meet both low modulus and printability requirements, representing a major challenge in the field of bioprinting. In this study, a low-modulus printable GelMA/Fib matrix bioink suitable for DIW printing processes and conducive to the spreading and growth of neural cells was developed. The experimental results indicated that changes in the GelMA component had a direct impact on the mechanical properties of the post-printed hydrogel blocks. Therefore, to ensure printability, the GelMA content should be reduced as much as possible. Conversely, the addition of fibrinogen significantly promoted the spreading of neural cells within the tissue block; however, increasing the fibrinogen content reduced the pore size of the hydrogel after formation, subsequently hindering the spreading of neural cells. Moreover, compared with pure GelMA, the mixed hydrogel added with Fib shows lower compression modulus. The addition of hydrogels such as sodium alginate [27] and heparin [28] will inhibit the formation of collagen hydrogel fiber network, resulting in the formation of small holes and poor collagen cross-linking, which will lead to the deterioration of its mechanical properties. Similarly, after adding Fib, a large number of smaller pores appeared in the pore wall of GelMA/Fib composite hydrogel (Fig. 5b), so it is inferred that Fib inhibited the formation of GelMA fiber network, which led to poor crosslinking of GelMA, thus reducing the compressive modulus of the composite hydrogel.

In this paper, a cross-layer continuous fiber structure was introduced into the proposed biomimetic cortical model as a topographical cue for inducing the orientation of neural neurites, whose impact of fiber structural size parameters on the oriented induction function of cells in post-printed tissues was systematically studied. There are two theories in the literature regarding the mechanisms of fiber topographical factors guiding cell orientation. The first mechanism suggests that the extension of neurites depends on the growth cones in neuronal cells, which contain a large number of receptors [29,30] capable of detecting topographical cues [31–36]. These receptors then activate focal adhesion kinases [37–39], which are highly related to cell adhesion and migration and can further initiate neurite growth in the direction of the fibers [40]. This was consistent with the experimental results obtained in this study. Since the diameter of fibers (10 μm) is close to the size of PC12 cells (10–20 μm), this enhances the effect of cell adhesion [19,20]. Therefore, the diameter of the fibers can significantly affect the orientation of the cells around them, with smaller-diameter fiber structures being more effective in guiding the orientation of neurites in neural cells. The second mechanism suggests that topographical cues can control the growth direction and length of nearby neurites along the fiber direction. In this

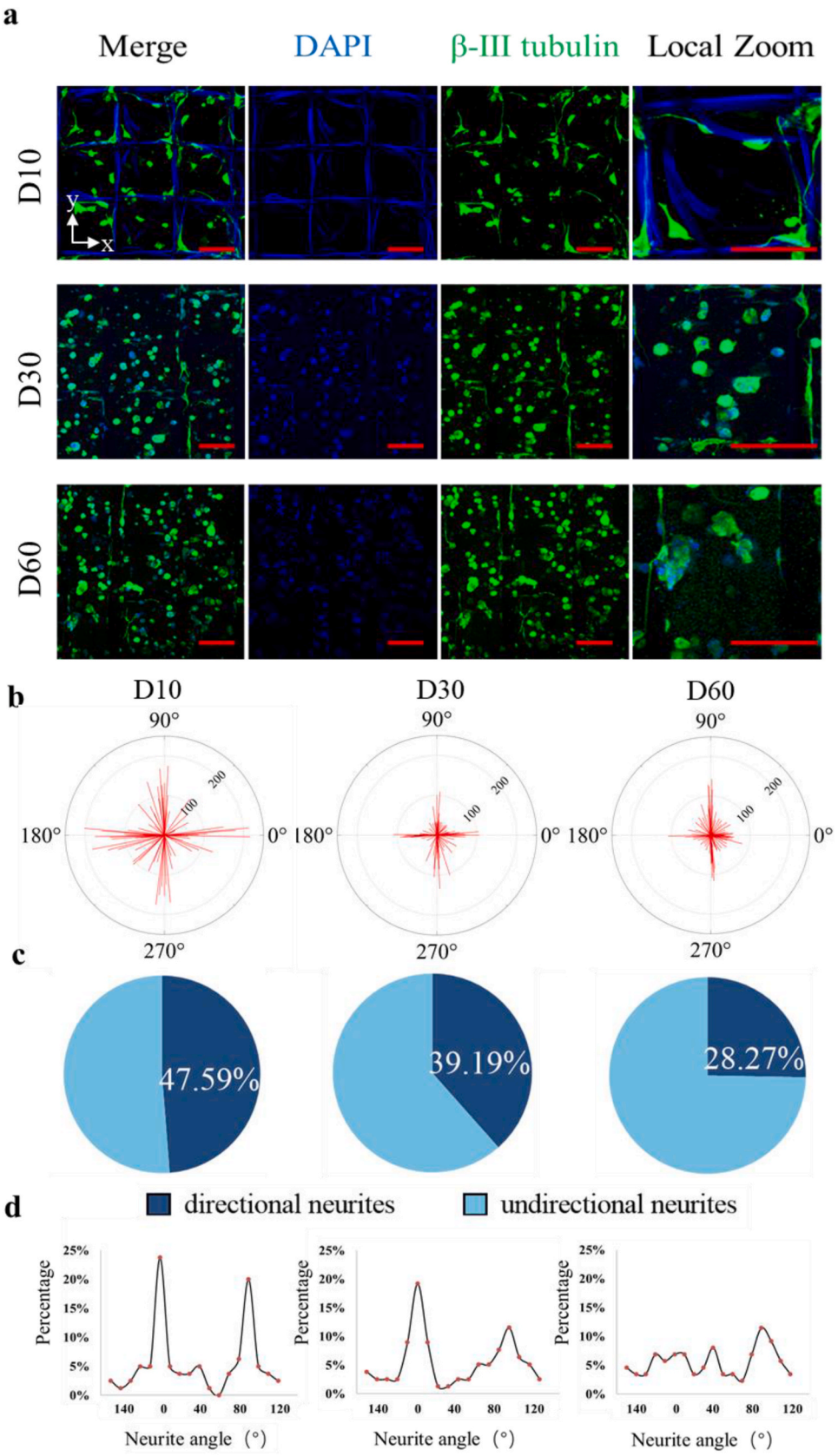

Fig. 6. The effect of fiber diameter to the cell morphology within the hydrogel/fiber composite tissue blocks (distance between fibers is 300 μm). (a) LSCM images of PC12 cells of group D10, D30 and D60 (scale bars = 200 μm); (b) The compass graphs of the neurite distribution in each group (red line's length represents the length of the neurite; and the line's angle represents the angle between the neurite and the x-axis in (a)); (c) Statistical ratio of the orientated and non-orientated neurite for each group; (d) Percentage distribution of the neurite against the x-axis in (a) in all groups.

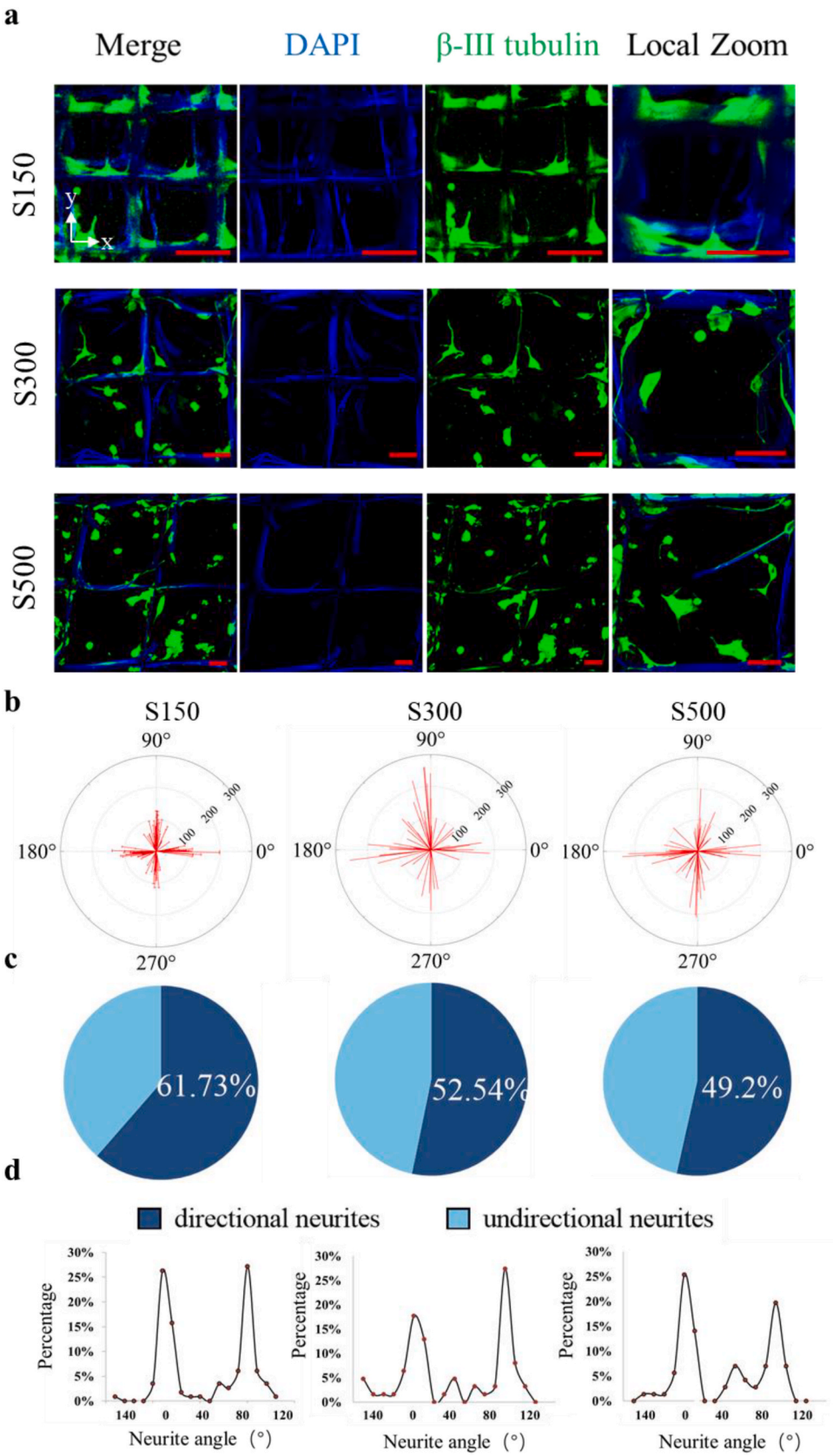

Fig. 7. The effect of fiber distance to the cell morphology within the hydrogel/fiber composite tissue blocks (fiber diameter is 10 μm). (a) LSCM images of PC12 cells of group S150, S300 and S500 (scale bars = 100 μm); (b) The compass graphs of the neurite distribution in group S150, S300 and S500 (red line's length represents the length of the neurite; and the line's angle represents the angle between the neurite and the x-axis in (a)); (c) Statistical ratio of the orientated and non-orientated neurite for each group; (d) Percentage distribution of the neurite against the x-axis in (a) in all groups.

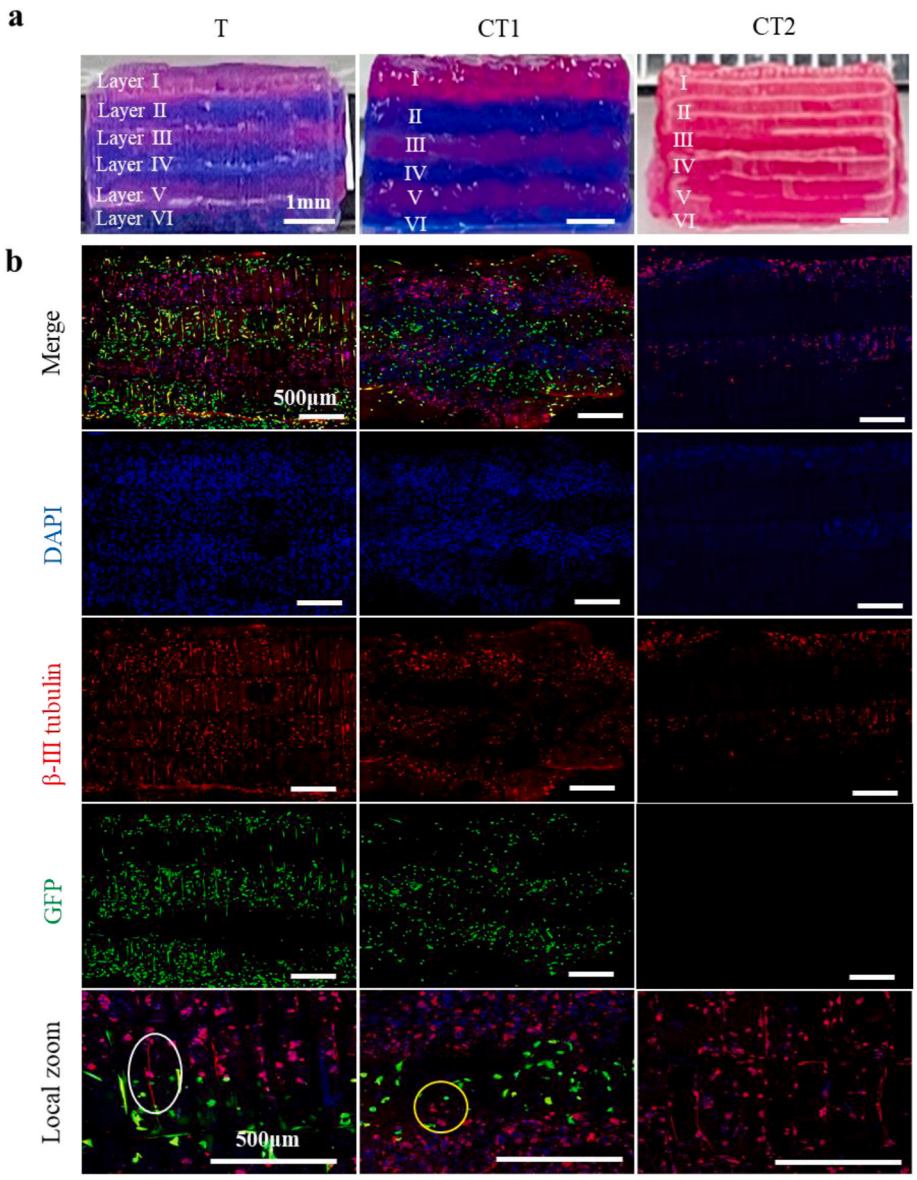

Fig. 8. The macro- and micro-structure of the printed biomimetic cortical model. (a) The photos of printed tissue samples of group T, CT1 and CT2; (b) The LSCM images of immunofluorescence-stained tissues for group T, CT1 and CT2 (blue: DAPI; red: β- III Tubulin of PC12; green: GFP in GL261; white circle: a typical extended neurite of PC12 into the GL261 cell layer; yellow circle: PC12 cells migrated into the GL261 cell layer).

study, an equilateral grid structure was used to lay out the fibers and the experimental results showed that the average length of neurites in the group with a fiber spacing of 150 μm was smaller than that of the other two groups with larger spacing (300 μm, 500 μm). This demonstrated the sensitivity of cell neurites to topographical cues during growth and development. In this study, smaller spacing (150 μm) increased the opportunity for cells to detect topographical cues, thereby promoting cells to activate contact-dependent and pathfinding mechanisms. Therefore, in subsequent models for the *in-vitro* construction of brain-like tissues, an appropriate spatial structure of topographical cues could be a useful tool for better control of the orientation and extension of neural cell neurites [41–43].

Furthermore, in the CT2 group with a layered structure without fibers, the majority of neural cells were spherical or irregular, with very few extended axons, and the length of cell protrusions did not exceed the size of their cell bodies (about 20~30 μm); whereas in the brain-like cortical model T group containing fibers and glial cell layers, 87 % of the neural cells were able to generate one or two branches symmetrically along the longitudinal direction of the fibers, displaying a more regular distribution. The length of cell protrusions around the fibers was ten times those in groups of structures without fibers (200–300 μm). Along with the tissue culture time, the glial cells in the tissue appeared elongated and spindle-shaped, adhering to the fibers. These results demonstrate that the "topographical" features created by the continuous fibers in the tissue can effectively promote the adhesion, migration, and growth of neurites of neural cells and can simulate the growth state of neural cells such as pyramidal cells and spindle cells in the real cortex, extending in a direction perpendicular to the cortical surface, which further enables functional connections of cell-cell and cell-matrix. This study provides an important experimental foundation for guiding and controlling the extension of neurites and connections in neural networks in later studies.

Neuroglial cells are normally considered support cells for neurons in the field of brain science. In the natural cortex, neuroglial cells [44] release neurotrophic factors [45] that guide neuronal migration. In the multilayer biomimetic cortical model constructed in this study, the glial cell and neuron layers were adjacent but separated. After 6 days of culture, PC12 cells migrated towards the glial cell layer, validating the

inductive and supportive role of neuroglial cells on neuronal cells [46–48] and emphasizing the importance of incorporating neuroglial cells into *in-vitro* 3D brain-like models. However, the presence of glial cells did not appear to have a significant effect on the extension of neural neurites [4].

Because of the presence of both horizontally and vertically aligned fibers in the biomimetic model proposed in this study, it was difficult to fully present the six-layer structure simultaneously during tissue sectioning and immunofluorescence staining. Therefore, only a five-layer structure composed of vertically oriented fibers was observed in the immunofluorescence staining images. Moreover, this study used PC12 and GL261 cell lines as substitutes for a variety of primary neuronal cells to verify the effectiveness of the printed structure, making it difficult to fully represent the biomimetic function of the cortical tissue model. In future work, induced pluripotent stem cells [6,49,50] should be combined with our proposed multi-scale model and bioprinting methods to construct an *in-vitro* biomimetic cortical model that is closer to a real situation, so as to study the development and the pathopharmacology of human brain.

The cells in the fiber spacing did not perform obvious orientation, because the mechanical and chemical properties of the bioink were still not completely matched with cells [51]. Besides, in the cortical model, the fibers spacing between two hydrogel layers was larger than 400 μm, which is limited by the thickness of the printing hydrogel layer, so the cells showed limited orientation and migration. In the future, the improvement of the material system and fiber manufacturing technology will bring better cell orientation and a more accurate brain cortex model.

5. Conclusion

A brain-like model with a biomimetic cortical structure was designed in this study, which included six layers comprising different cellular components and microscale continuous fibers running vertically through all the layers. A multimaterial composite printing/culturing integrated bioprinting platform was developed in-house, incorporating two 3D printing technologies: DIW of cell-laden hydrogels and EHD of fibers. Based on the integrated 3D printing technology and the developed low-modulus bioink, a designed biomimetic brain-like tissue model was fabricated, and the influence of macroscopic and microscopic structural features on the orientation of neural neurites as well as the interaction between cells and the matrix was systematically investigated in a 3D manner. Morphological connections between neurons across the layers were observed in the fabricated *in-vitro* biomimetic cortical models. Micro-scale (10 μm) cross-layer fibers effectively guided and controlled the extension length and direction of the neurites of surrounding neurons but had negligible effects on the migration of neurons; whereas glial cells significantly promoted the migration of surrounding PC12 cells but had negligible effects on the extension of neurites. This study provides an important foundation for the design and fabrication of precise brain-like models with functional neuronal connections.

CRediT authorship contribution statement

Ling Wang: Writing – original draft, Conceptualization. **Luge Bai:** Writing – original draft, Investigation. **Sen Wang:** Investigation. **Jiajia Zhou:** Investigation. **Yingjie Liu:** Methodology. **Chenrui Zhang:** Methodology. **Siqi Yao:** Methodology. **Jiankang He:** Methodology. **Chaozong Liu:** Methodology. **Dichen Li:** Conceptualization.

Declaration of competing interest

The authors declare that they have no known competing financial interests or personal relationships that could have appeared to influence the work reported in this paper.

Data availability

Data will be made available on request.

Acknowledgements

This work was supported by the Program of the National Natural Science Foundation of China [52275291]; the Program for Innovation Team of Shaanxi Province [2023-CX-TD-17]; and the Fundamental Research Funds for the Central Universities.

Appendix A. Supplementary data

Supplementary data to this article can be found online at https://doi.org/10.1016/j.mtbio.2024.101176.

References

[1] M. Segel, B. Neumann, M.F.E. Hill, et al., Niche stiffness underlies the ageing of central nervous system progenitor cells, Nature 573 (2019) 130–134, https://doi.org/10.1038/s41586-019-1484-9.
[2] S. Herculano-Houzel, The glia/neuron ratio: how it varies uniformly across brain structures and species and what that means for brain physiology and evolution, Glia 62 (2014) 1377–1391, https://doi.org/10.1002/glia.22683.
[3] J. Yin, M. Yan, Y. Wang, et al., 3D bioprinting of low-concentration cell-laden gelatin methacrylate (GelMA) bioinks with a two-step cross-linking strategy, ACS Appl. Mater. Interfaces 10 (2018) 6849–6857, https://doi.org/10.1021/acsami.7b16059.
[4] L. Bai, Z. Hao, S. Wang, et al., Biomimetic three-dimensional glioma model printed in vitro for the studies of glioma cells and neurons interactions, International Journal of Bioprinting 9 (2023), https://doi.org/10.18063/ijb.715.
[5] Y.-T.L. Dingle, M.E. Boutin, A.M. Chirila, et al., Three-dimensional neural spheroid culture: AnIn VitroModel for cortical studies, Tissue Eng. C Methods 21 (2015) 1274–1283, https://doi.org/10.1089/ten.tec.2015.0135.
[6] S. Velasco, A.J. Kedaigle, S.K. Simmons, et al., Individual brain organoids reproducibly form cell diversity of the human cerebral cortex, Nature 570 (2019) 523–527, https://doi.org/10.1038/s41586-019-1289-x.
[7] C. Gonzalez, E. Armijo, J. Bravo-Alegria, et al., Modeling amyloid beta and tau pathology in human cerebral organoids, Mol. Psychiatr. 23 (2018) 2363–2374, https://doi.org/10.1038/s41380-018-0229-8.
[8] M. Kato-Negishi, Y. Morimoto, H. Onoe, et al., Millimeter-sized neural building blocks for 3D heterogeneous neural network assembly, Adv. Healthcare Mater. 2 (2013) 1564–1570, https://doi.org/10.1002/adhm.201300052.
[9] K. Chwalek, M.D. Tang-Schomer, F.G. Omenetto, et al., In vitro bioengineered model of cortical brain tissue, Nat. Protoc. 10 (2015) 1362–1373, https://doi.org/10.1038/nprot.2015.091.
[10] S. Bang, S. Na, J.M. Jang, et al., Engineering-aligned 3D neural circuit in microfluidic device, Adv. Healthcare Mater. 5 (2016) 159–166, https://doi.org/10.1002/adhm.201500397.
[11] S.V. Murphy, A. Atala, 3D bioprinting of tissues and organs, Nat. Biotechnol. 32 (2014) 773–785, https://doi.org/10.1038/nbt.2958.
[12] Murat Guvendiren (Ed.), 3D Bioprinting in Medicine: Technologies, Bioinks, and Applications, Springer, 2019.
[13] Y. Song, X. Su, K.F. Firouzian, et al., Engineering of brain-like tissue constructs via 3D Cell-printing technology, Biofabrication 12 (2020) 035016, https://doi.org/10.1088/1758-5090/ab7d76.
[14] R. Lozano, L. Stevens, B.C. Thompson, et al., 3D printing of layered brain-like structures using peptide modified gellan gum substrates, Biomaterials 67 (2015) 264–273, https://doi.org/10.1016/j.biomaterials.2015.07.022.
[15] Y.E. Li, Y.A. Jodat, R. Samanipour, et al., Toward a neurospheroid niche model: optimizing embedded 3D bioprinting for fabrication of neurospheroid brain-like co-culture constructs, Biofabrication 13 (2020), https://doi.org/10.1088/1758-5090/abc1be.
[16] C.-Y. Yang, W.-Y. Huang, L.-H. Chen, et al., Neural tissue engineering: the influence of scaffold surface topography and extracellular matrix microenvironment, J. Mater. Chem. B 9 (2021) 567–584, https://doi.org/10.1039/d0tb01605e.
[17] E.J. Berns, S. Sur, L. Pan, et al., Aligned neurite outgrowth and directed cell migration in self-assembled monodomain gels, Biomaterials 35 (2014) 185–195, https://doi.org/10.1016/j.biomaterials.2013.09.077.
[18] J. Zhang, X. Zhang, C. Wang, et al., Conductive composite fiber with optimized alignment guides neural regeneration under electrical stimulation, Adv. Healthcare Mater. 10 (2020), https://doi.org/10.1002/adhm.202000604.
[19] H. Hajiali, A. Contestabile, E. Mele, et al., Influence of topography of nanofibrous scaffolds on functionality of engineered neural tissue, J. Mater. Chem. B 6 (2018) 930–939, https://doi.org/10.1039/c7tb02969a.
[20] Z. Zhang, M.L. Jørgensen, Z. Wang, et al., 3D anisotropic photocatalytic architectures as bioactive nerve guidance conduits for peripheral neural regeneration, Biomaterials 253 (2020), https://doi.org/10.1016/j.biomaterials.2020.120108.

[21] S.-J. Lee, M. Nowicki, B. Harris, et al., Fabrication of a highly aligned neural scaffold via a table top stereolithography 3D printing and electrospinning, Tissue Eng. 23 (2017) 491–502, https://doi.org/10.1089/ten.tea.2016.0353.
[22] R.H.S. Westerink, A.G. Ewing, The PC12 cell as model for neurosecretion, Acta Physiol. 192 (2007) 273–285, https://doi.org/10.1111/j.1748-1716.2007.01805.x.
[23] C. Malagelada, L. Greene, Parkinson's Disease: Molecular and Therapeutic Insights from Experimental models[J], 2008.
[24] A.I. Van Den Bulcke, B. Bogdanov, N. De Rooze, et al., Structural and rheological properties of methacrylamide modified gelatin hydrogels, Biomacromolecules 1 (1) (2000) 31–38, https://doi.org/10.1021/bm990017d.
[25] Y. Wu, Y. Xiang, J. Fang, et al., The influence of the stiffness of GelMA substrate on the outgrowth of PC12 cells, Biosci. Rep. 39 (2019), https://doi.org/10.1042/bsr20181748.
[26] M. Cadena, L. Ning, A. King, et al., 3D bioprinting of neural tissues, Adv. Healthcare Mater. 10 (2020), https://doi.org/10.1002/adhm.202001600.
[27] B.M. Gillette, J.A. Jensen, B. Tang, et al., In situ collagen assembly for integrating microfabricated three-dimensional cell-seeded matrices, Nat. Mater. 7 (2008) 636–640, https://doi.org/10.1038/nmat2203.
[28] A.O. Brightman, B.P. Rajwa, J.E. Sturgis, et al., Time-lapse confocal reflection microscopy of collagen fibrillogenesis and extracellular matrix assembly in vitro, Biopolymers: Original Research on Biomolecules 54 (3) (2000) 222–234.
[29] M. Tessier-Lavigne, C.S. Goodman, The molecular biology of axon guidance, Science 274 (5290) (1996) 1123–1133, https://doi.org/10.1126/science.274.5290.1123.
[30] M. Marcus, K. Baranes, M. Park, et al., Interactions of neurons with physical environments, Adv. Healthcare Mater. 6 (2017), https://doi.org/10.1002/adhm.201700267.
[31] K. Franze, The mechanical control of nervous system development, Biophys. J. 112 (2017), https://doi.org/10.1016/j.bpj.2016.11.029.
[32] O.V. Cangellaris, M.U. Gillette, Biomaterials for enhancing neuronal repair, Frontiers in Materials 5 (2018), https://doi.org/10.3389/fmats.2018.00021.
[33] L.S. Zweifel, R. Kuruvilla, D.D. Ginty, Functions and mechanisms of retrograde neurotrophin signalling, Nat. Rev. Neurosci. 6 (2005) 615–625, https://doi.org/10.1038/nrn1727.
[34] E.W. Dent, F.B. Gertler, Cytoskeletal dynamics and transport in growth cone motility and axon guidance, Neuron 40 (2) (2003) 209–227, https://doi.org/10.1016/S0896-6273(03)00633-0.
[35] S. Geraldo, P.R. Gordon-Weeks, Cytoskeletal dynamics in growth-cone steering, J. Cell Sci. 122 (2009) 3595–3604, https://doi.org/10.1242/jcs.042309.
[36] B.T. Schaar, S.K. McConnell, Cytoskeletal coordination during neuronal migration, Proc. Natl. Acad. Sci. USA 102 (38) (2005) 13652–13657, https://doi.org/10.1073/pnas.0506008102.
[37] H. Yuan, Q. Zhou, B. Li, et al., Direct printing of patterned three-dimensional ultrafine fibrous scaffolds by stable jet electrospinning for cellular ingrowth, Biofabrication 7 (2015), https://doi.org/10.1088/1758-5090/7/4/045004.
[38] M. Castilho, D. Feyen, M. Flandes-Iparraguirre, et al., Melt electrospinning writing of poly-hydroxymethylglycolide-co-ε-caprolactone-based scaffolds for cardiac tissue engineering, Adv. Healthcare Mater. 6 (2017), https://doi.org/10.1002/adhm.201700311.
[39] J. Wang, H. Wang, X. Mo, et al., Reduced graphene oxide-encapsulated microfiber patterns enable controllable formation of neuronal-like networks, Adv Mater 32 (2020) e2004555, https://doi.org/10.1002/adma.202004555.
[40] A.N. Koppes, N.W. Zaccor, C.J. Rivet, et al., Neurite outgrowth on electrospun PLLA fibers is enhanced by exogenous electrical stimulation, J. Neural. Eng. 11 (2014), https://doi.org/10.1088/1741-2560/11/4/046002.
[41] Y. Li, Y. Xiao, C. Liu, The horizon of materiobiology: a perspective on material-guided cell behaviors and tissue engineering, Chem. Rev. 117 (2017) 4376–4421, https://doi.org/10.1021/acs.chemrev.6b00654.
[42] A. Higuchi, Q.-D. Ling, Y. Chang, et al., Physical cues of biomaterials guide stem cell differentiation fate, Chem. Rev. 113 (2013) 3297–3328, https://doi.org/10.1021/cr300426x.
[43] Z. Zhang, Y. Wang, Z. Chen, et al., Tailoring conductive inverse opal films with anisotropic elliptical porous patterns for nerve cell orientation, J Nanobiotechnology 20 (2022) 117, https://doi.org/10.1186/s12951-022-01340-w.
[44] G.M. Smith, R.H. Miller, J. Silver, Changing role of forebrain astrocytes during development, regenerative failure, and induced regeneration upon transplantation, J. Comp. Neurol. 251 (1) (1986) 23–43, https://doi.org/10.1002/cne.902510103.
[45] H. Müller, Astroglial neurotrophic and neurite-promoting factors, Pharmacology & Therapeutics 65 (1) (1995) 1–18, https://doi.org/10.1016/0163-7258(94)00047-7.
[46] J.E. Collazos-Castro, C. García-Rama, A. Alves-Sampaio, Glial progenitor cell migration promotes CNS axon growth on functionalized electroconducting microfibers, Acta Biomater. 35 (2016) 42–56, https://doi.org/10.1016/j.actbio.2016.02.023.
[47] A.V. Molofsky, K.W. Kelley, H.-H. Tsai, et al., Astrocyte-encoded positional cues maintain sensorimotor circuit integrity, Nature 509 (2014) 189–194, https://doi.org/10.1038/nature13161.
[48] S. Kidambi, I. Lee, C. Chan, Primary neuron/astrocyte Co-culture on polyelectrolyte multilayer films: a template for studying astrocyte-mediated oxidative stress in neurons, Adv. Funct. Mater. 18 (2008) 294–301, https://doi.org/10.1002/adfm.200601237.
[49] G. Quadrato, T. Nguyen, E.Z. Macosko, et al., Cell diversity and network dynamics in photosensitive human brain organoids, Nature 545 (2017) 48–53, https://doi.org/10.1038/nature22047.
[50] M.A. Lancaster, J.A. Knoblich, Organogenesis in a dish: modeling development and disease using organoid technologies, Science 345 (2014), https://doi.org/10.1126/science.1247125.
[51] E. Axpe, G. Orive, K. Franze, et al., Towards brain-tissue-like biomaterials, Nat. Commun. 11 (2020) 3423, https://doi.org/10.1038/s41467-020-17245-x.